

# An Artificial Intelligence based approach for constraining the redshift of blazars using $\gamma$ -ray observations

K K Singh<sup>a,b</sup>, V K Dhar<sup>b</sup>, P J Meintjes<sup>a</sup>

<sup>a</sup>*Physics Department, University of the Free State, Bloemfontein- 9300, South Africa*

<sup>b</sup>*Astrophysical Sciences Division, Bhabha Atomic Research Center, Mumbai- 400 085, India*

---

## Abstract

In this paper, we discuss an artificial intelligence based approach to constrain the redshift of blazars using combined  $\gamma$ -ray observations from the *Fermi* Large Area Telescope (LAT) and ground based atmospheric Cherenkov telescopes (ACTs) in GeV and *sub* TeV energy regimes respectively. The spectral measurements in GeV and TeV energy bands show a redshift dependent spectral break in the  $\gamma$ -ray spectra of blazars. We use this observational feature of blazars to constrain their redshift. The observed spectral information of blazars with known redshifts reported in the *Fermi* catalogs (3FGL and 1FHL) and TeV catalog are used to train an Artificial Neural Network (ANN) based algorithm. The training of the ANN methodology is optimized using *Levenberg - Marquardt* algorithm with  $\gamma$ -ray spectral indices and redshifts of 35 well observed blazars as input and output parameters respectively. After training, we use only observed spectral indices in GeV and sub TeV regimes for 10 blazars as inputs to predict their redshifts. The

---

*Email address:* kksastro@barc.gov.in (K K Singh)

comparison of predicted redshifts by the ANN with the known redshift suggests that both the values are consistent within  $\sim 18\%$  uncertainty. The method proposed in the present work would be helpful in future for constraining or predicting the redshifts of the blazars using only observational  $\gamma$ -ray spectral informations obtained from the *Fermi*-LAT and current generation IACTs as well as from the next generation Cherenkov Telescope Array (CTA) with improved source statistics.

*Keywords:* Blazars: distances and redshifts, radiation mechanisms: non-thermal, Gamma-rays: general

---

## 1. Introduction

Blazars are radio-loud Active Galactic Nuclei (AGN) constituting a major population of the TeV  $\gamma$ -ray sources in the extragalactic Universe. These sources are characterized by a supermassive black hole surrounded by an accretion disk at the center of a host galaxy with generally elliptical morphology and a relativistic jet pointing towards the observer at Earth [1]. The orientation of the jet close to the line of sight of the observer leads to the relativistic beaming effects like superluminal motion and strong anisotropic radiation in the non-thermal emission from the outflowing plasma. The observed luminosity from such sources outshines their host galaxy and the non-thermal continuum emission from the jet can extend over the entire electromagnetic spectrum from radio to very high energy (VHE:  $E > 100$  GeV)  $\gamma$ -ray. The strong non-thermal emission characterizes the broad-band spectral energy distribution (SED) of blazars with two characteristic

humps peaking at low and high energies (HE:  $E > 100$  MeV) respectively. The origin of the low energy hump from radio to X-rays through optical/UV is attributed to the synchrotron emission from the relativistic electrons gyrating in the magnetic field of the jet. The synchrotron origin of low energy component in the blazar SED is completely understood and has been observationally supported by the measurements of the high degree of linear polarization in radio and optical bands [2, 3]. The physical mechanism for the second component from MeV-GeV to VHE or TeV  $\gamma$ -rays is not very clear and various models based on the leptonic and hadronic processes have been proposed in the literature [4, 5, 6, 7].

Based on the position of the synchrotron peak in the low energy hump of the SED, blazars are classified as low-synchrotron peaked (LSP), intermediate-synchrotron peaked (ISP) and high-synchrotron peaked (HSP) sources [8]. For LSP blazars, the rest frame synchrotron peak frequency is lower than  $10^{14}$  Hz and ISP sources have peak frequency in the range  $10^{14}$  Hz to  $10^{15}$  Hz. The synchrotron peak frequency for HSP blazars is generally observed to be more than  $10^{15}$  Hz and up to  $10^{18}$  Hz for specific sources. According to Meyer et al. (2011), HSP blazars and radio galaxies of FR I type have weak relativistic jets whereas LSP blazars and FR II radio galaxies belong to the strong jet population [9]. Blazars are also classified as BL Lacertae objects (BL Lacs) and Flat Spectrum Radio Quasars (FSRQs) on the basis of their properties in the optical band [10]. The optical radiation from blazars is considered to have contributions from both thermal and non-thermal emissions. The thermal emission originates from the accretion onto the supermassive black hole and from the host galaxy of the source. The

non-thermal contribution comes from the relativistic jet. The optical spectra of FSRQs show strong emission lines from the thermal plasma contribution whereas no or weak emission lines are observed from the BL Lacs. This indicates that the host galaxy features are not clearly visible in the optical spectra of BL Lacs as compared to the FSRQs. The observed blazar sequence (anticorrelation between bolometric luminosity and synchrotron peak frequency) suggests that FSRQs are high power LSP blazars whereas BL Lacs are low power HSP sources [11].

The featureless optical spectra of BL Lacs render serious challenges in the measurement of their redshift ( $z$ ) using optical spectroscopic methods. The redshift of cosmic sources like blazars is one of the important concepts of astrophysics and can be measured directly in observational cosmology. It plays a very important role in probing the evolution and structure formation in the Universe. In particular, the evolutionary properties of blazars is an open question in AGN astrophysics and cosmology. Apart from the cosmological evolution, the redshift of blazars is crucial for interpreting their multi-wavelength emission with different models and to study the intergalactic magnetic field (IGMF) and extragalactic background light (EBL) using  $\gamma\gamma$ -interactions via pair production. Despite many optical spectroscopic campaigns for measuring the redshift of blazars, only a small fraction of BL Lacs have well known redshifts [12, 13, 14]. However, redshift measurements of a large fraction of FSRQs using spectroscopic observations have been reported [15]. A new physical method for the measurement of redshift of AGN using the time lag between light curves in high and low energy bands is also proposed [16]. This method is based on the quantitative model of the dust

reverberation in AGN which relates the absolute luminosity of the source with the time lag but it is useful for sources at smaller redshifts only. Prandini et al. (2010) have pioneered a method to constrain the redshift of blazars using combined GeV-TeV  $\gamma$ -ray observations [17]. This method strongly depends on the model for the density of EBL photons in the Universe which is not exactly known until today [18, 19, 20, 21] and use of different EBL models which may lead to large uncertainty in the derived redshift for a given source. Another method proposed by Qin et al. (2018) estimates redshift of three BL Lacs through the fitting of their broadband SED using a single zone leptonic model [22]. This method also depends on the EBL model and the model for multi-wavelength emission from blazars which are not universally applicable to all sources.

In this work, we propose an artificial intelligence based approach using Artificial Neural Network (ANN) to constrain the redshift of blazars from the GeV-TeV  $\gamma$ -ray observations. This method is based on the assumption that the observed spectral-break between MeV-GeV spectra from the *Fermi*-Large Area Telescope (LAT) and TeV spectra from the ground-based observations of blazars strongly depends on the redshift of the source. Such a correlation could arise, for example, because of attenuation of TeV photons by EBL during their propagation towards Earth. The paper is structured as following: in Section 2, we discuss the  $\gamma$ -ray spectra of blazars. The blazar sample used in this work is described in Section 3. In Section 4, a brief description of the ANN methodology is presented. The results are discussed in Section 5. Finally, we have summarized the study in Section 6.

Table 1: List of blazars selected for ANN training from the TeGeV/TeV catalog with known redshift.

Name	Type	Redshift (z)
PKS 2005-489	HSP	0.071
H 2356-309	HSP	0.165
Mrk 180	HSP	0.045
PKS 0548-322	HSP	0.069
1ES 1011+496	HSP	0.212
RGB J0152+017	HSP	0.08
1ES 0806+524	HSP	0.138
RGB J0710+591	HSP	0.125
RBS 0413	HSP	0.19
1H 0323+022	HSP	0.147
VER 0648+152	HSP	0.179
B3 2247+381	HSP	0.1187
1RXS J1010-311	HSP	0.1426
1ES 1727+502	HSP	0.055
1ES 0120+340	HSP	0.272
Mrk 421	HSP	0.031
1ES 1741+196	HSP	0.084
H 1426+428	HSP	0.129
1ES 1959+650	HSP	0.048
PKS 2155-304	HSP	0.116
1ES 1218+304	HSP	0.182
1ES 1101-232	HSP	0.186
1ES 0033+595	HSP	0.086
TXS 1055+567	HSP	0.143
1H 0658+595	HSP	0.125
PKS 0301-243	HSP	0.266
1H 1013+498	HSP	0.212
3C 66A	ISP	0.444
VER J0521+211	ISP	0.108
S5 0716+714	ISP	0.31
1ES 2202+420	ISP	0.069
AP Librae	LSP	0.049
3C 279	LSP	0.5362
PKS 1222+21	LSP	0.432
PKS 1510-089	LSP	0.361

## 2. GeV-TeV $\gamma$ -ray Spectra of Blazars

The origin of  $\gamma$ -ray emission from blazars has not been completely understood so far and it is attributed to the inverse Compton (IC) scattering of low energy photons by the relativistic electrons in the leptonic scenario and to the synchrotron radiation of ultrarelativistic protons in the hadronic models [23]. However, the  $\gamma$ -ray observations of blazars suggest that the observed  $\gamma$ -ray emission from most of the blazars can be described by a power law in a given energy range. Therefore, the differential spectrum of  $\gamma$ -ray photons observed from a blazar by an instrument can be expressed as

$$F_{obs}(E) \propto E^{-\Gamma} \quad (1)$$

where  $\Gamma$  is the power law spectral index. The *Fermi*-Large Area Telescope (LAT) provides an excellent measurement of  $\Gamma$  in the GeV energy band where the peak of the HE component in the SED is observed for most of the blazars [24]. For  $\Gamma \leq 2$ , the *Fermi*-LAT detects the photons with energy less than the peak energy of the HE component in the broad-band SED, which is generally referred to as the hard spectrum. The observations with the ground-based atmospheric Cherenkov telescopes measure the spectral index of TeV photons in the VHE regime, which belongs to the soft or steep portion of the spectrum. Therefore, the observations from the *Fermi*-LAT overlapping with the ground-based observations can provide a good shape of the  $\gamma$ -ray spectra of blazars in the GeV-TeV energy range and also the peak of HE component in SED.

Table 2: Summary of the blazar sample from the TeGeV/TeV catalog used for testing ANN.

Name	Type	z(Known)	z(ANN)	Uncertainty in z (%)
1ES 0502+675	HSP	0.341	0.358	4.98
Mrk 501	HSP	0.034	0.040	17.60
1ES 0647+250	HSP	0.203	0.206	1.47
1ES 1440+122	HSP	0.162	0.156	3.70
1ES 2344+514	HSP	0.044	0.049	11.36
PKS 0447-439	HSP	0.343	0.329	4.08
1ES 1312-423	HSP	0.105	0.107	1.90
PG 1553+113	HSP	0.129	0.131	1.55
B2 1219+28	ISP	0.102	0.103	0.98
1ES 1215+303	LSP	0.130	0.110	15.38

### 3. The Blazar Sample

The launch of Large Area Telescope (LAT) onboard the *Fermi* satellite in 2008 has opened a new window to explore the  $\gamma$ -ray sky using space-based observations in the GeV energy band [24]. The *Fermi*-LAT observations combined with the ground-based Cherenkov telescopes operating in sub-TeV energy range provide an unique opportunity to obtain a number of innovative scientific results in astrophysics and cosmology. Based on the first four years of data taken during August 2008 to July 2012, more than 1100 blazars have been reported in the third *Fermi*-LAT source catalog (3FGL) in the energy range 0.1-300 GeV [25]. The first *Fermi*-LAT catalog of high energy sources above 10 GeV (1FHL) describes more than 300 blazars detected in the energy range 10 GeV–500 GeV using first three years of data from August 2008 to August 2011 [26]. The  $\gamma$ -ray emission from the majority of the blazars reported in the 3FGL and 1FHL catalogs is described



by a power law in the energy bands 0.1-300 GeV and 10-500 GeV respectively. The combined observations from the 3FGL and 1FHL catalogs provide an important data set to determine the HE  $\gamma$ -ray spectra of blazars in the wide energy range of 0.1-500 GeV. However, more than 50% of the blazars reported in these catalogs lack their redshift measurements. The online TeGeV catalog [27] and TeV catalog<sup>1</sup> provide results from the VHE  $\gamma$ -ray observations of the sources by the past and current generation of ground-based Cherenkov telescope. More than 70 blazars have been discovered at TeV energies in the extragalactic Universe by the ground-based Cherenkov telescopes. An interactive version of the above three catalogs (3FGL, 1FHL and TeGeV) is publicly available at Space Science Data Center (SSDC)<sup>2</sup>. This provides a very useful quasi-simultaneous data base of blazars in three  $\gamma$ -ray energy bands. The redshift measurements of these sources using optical observations suggest that most of the TeV blazars are located at redshift  $z < 1$ . BL Lac blazars are observed at low redshifts while FSRQs have relatively higher redshift [11]. In the present work, we have selected a sample of 45 blazars from the TeGeV or TeV catalog with their  $\gamma$ -ray spectral measurements available in 3FGL and 1FHL catalogs. The  $\gamma$ -ray spectra of blazars selected in the sample are described by a power law with spectral indices  $\Gamma_{TeV}$ ,  $\Gamma_{3FGL}$  and  $\Gamma_{1FHL}$  in the TeV, 3FGL and 1FHL catalogs respectively. We have randomly classified the blazar sample in two groups: training and testing data sets. A large fraction of the blazars with known redshift from this sample is used for training

---

<sup>1</sup><http://tevcat.uchicago.edu/>

<sup>2</sup><https://fermi.ssdsc.asi.it/>

the ANN methodology based on the spectral measurements of these source. The list of TeV blazars ( $\sim 35$ ) used for training the ANN is given in Table 1. About 10 blazars with well known redshifts are used as testing data set to validate the procedure for predicting the unknown redshift using their  $\gamma$ -ray spectral measurements from *Fermi*-LAT and TeV instruments. The blazar sample used for testing ANN is summarized in Table 2. It is important to note that few blazars in the sample have more than one redshift measurements in the literature. For such blazars, we have used only those redshift values which are commonly reported in various  $\gamma$ -ray catalogs in this study. Also, the spectral properties of blazars detected by the *Fermi*-LAT suggest that the distribution of power law spectral index of photons in the energy range above 100 MeV is strongly correlated with the blazar types [28]. A departure from the single power law photon spectrum is mainly observed for ISP and LSP types of blazars whereas this feature is absent in the HSP class of blazars. Therefore, we have selected only those *Fermi*-LAT blazars in the sample which are described by a single power law in MeV-GeV and TeV energy bands. The distribution of  $\gamma$ -ray spectral indices ( $\Gamma_{TeV}$ ,  $\Gamma_{3FGL}$  and  $\Gamma_{1FHL}$ ) of the blazar sample as a function of their known redshift ( $z$ ) is shown in Figure 1. It is evident from Figure 1 that most of the blazars in the sample are populated up to the redshift  $z < 0.3$  and the measured  $\gamma$ -ray spectral indices from the TeV instruments ( $\Gamma_{TeV}$ ) show a definite correlation with the redshift.

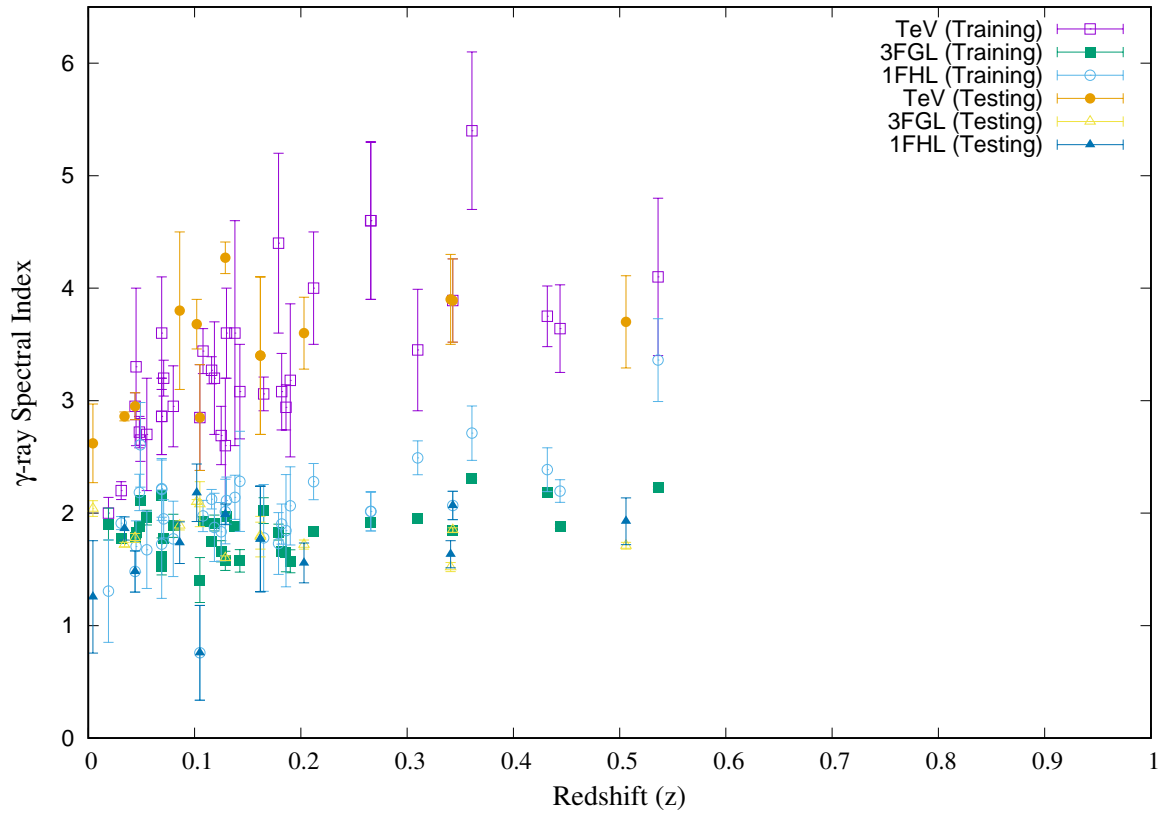


Figure 1:  $\gamma$ -ray spectral indices as a function of redshift for the sample of blazars selected for ANN training and testing.

#### **4. Artificial Neural Networks**

The artificial neural network (ANN) is a mathematical construct for data prediction by recognising the correlations and patterns in the input training data sets. The ANN based computational techniques efficiently replicate the behavior of human brain. ANN is collection of interconnected processing units known as nodes similar to the human brain which consists of biological cells called neurons. The strength of interconnection among neurons is characterized by weights. A neuron in the network generates a single output from multiple inputs. The ANN system has at least three layers namely input, output and hidden with different number of neurons. More than one hidden layer can also be used depending on the complexity of the problem. The hidden layer links input and output layers in a very complex way. In the simplest form, the data is supplied to the input layer neurons which generally acts as a buffer and passes the data to the hidden layer. The hidden layer produces an output using the non-linear transformations of the signal from the input layer and passes the data to the output layer to predict the output. The output generated by the ANN is compared with the desired output to estimate the error [29]. The ANN method learns by adjusting the weights such that the produced error is reduced until the final output is computed [30]. The number of neurons in a network is optimized from the nature of the problem at hand. The performance of an ANN as a whole is optimized using input training data sets with correct output for a given application. The first technique using artificial neurons was developed in 1943 to perform the logical operations [31]. Nowadays ANN based computational techniques have received ample applications in astrophysics,

science and other diverse areas.

#### *4.1. Training of ANN: Levenberg-Marquardt Method*

The training of ANN includes the search for appropriate values of network parameters by minimizing the difference between the predicted and correct values also known as the error function. A feed-forward method is the most commonly used ANN algorithm. However, varied algorithms exist under the ANN domain depending upon the choice of error function [32]. The learning schemes followed by Back-propagation based on the gradient-descent methods have several limitations [33]. In the gradient-based algorithms, it is difficult to obtain a unique set of optimal parameters due to the existence of multiple local minima. On the other hand, the Levenberg-Marquardt method is a compromise between the Newton method and the gradient descent method employed by the backpropagation algorithm. The advantage of this coalition is that while the Newton method converges very rapidly near a local or the global minimum but may also diverge, the gradient descent is assured of convergence through a proper selection of the step size, but converges slowly. For example, consider the optimization of a second order function  $F(\mathbf{w})$  and let  $\mathbf{g}$  and  $\mathbf{H}$  be the gradient vector and the Hessian respectively. According to the Levenberg-Marquardt method, the optimum adjustment  $\Delta\mathbf{w}$  applied to the parameter  $\mathbf{w}$  is defined as

$$\Delta\mathbf{w} = [\mathbf{H} + \lambda\mathbf{I}]^{-1} \mathbf{g} \quad (2)$$

where  $\mathbf{I}$  is the identity matrix of the same dimension as  $\mathbf{H}$  and  $\Lambda$  is a regularizing, loading/blending parameter that forces the sum matrix  $[\mathbf{H} + \Lambda\mathbf{I}]$  to be positive definite and well conditioned throughout the computation. Now considering the application to the present work which has a single output redshift ( $z$ ), the network is trained by minimizing the cost or the error function

$$\Omega_{av}(\mathbf{w}) = \frac{1}{2N} \sum_{i=1}^N [d(i) - F(\mathbf{x}(i), \mathbf{w})]^2 \quad (3)$$

where  $(\mathbf{x}(i), d(i))$  is the training sample comprising of spectral indices  $\Gamma_{TeV}$ ,  $\Gamma_{3FGL}$ ,  $\Gamma_{1FHL}$  and redshift ( $z$ ).  $F(\mathbf{x}(i), \mathbf{w})$  is the approximating function realized by the network. The synaptic weights of the network are arranged in some orderly manner to form the weight vector  $\mathbf{w}$ . The gradient and the Hessian of the error function  $\Omega_{av}(\mathbf{w})$  to be minimized are respectively defined as

$$\mathbf{g}(w) = \frac{\partial \Omega_{av}(\mathbf{w})}{\partial \mathbf{w}} = -\frac{1}{N} \sum_{i=1}^N [d(i) - F(\mathbf{x}(i), \mathbf{w})] \frac{\partial F(\mathbf{x}(i), \mathbf{w})}{\partial \mathbf{w}} \quad (4)$$

and

$$\mathbf{H}(\mathbf{w}) = \frac{\partial^2 \Omega_{av}(\mathbf{w})}{\partial \mathbf{w}^2} = \frac{1}{N} \sum_{i=1}^N \left[ \frac{\partial F(\mathbf{x}(i), \mathbf{w})}{\partial \mathbf{w}} \right] \left[ \frac{\partial F(\mathbf{x}(i), \mathbf{w})}{\partial \mathbf{w}} \right]^T \quad (5)$$

$$= -\frac{1}{N} \sum_{i=1}^N [d(i) - F(\mathbf{x}(i), \mathbf{w})] \frac{\partial^2 F(\mathbf{x}(i), \mathbf{w})}{\partial \mathbf{w}^2} \quad (6)$$

Substituting the solutions obtained for above equations in the equation 2, the desired weight adjustment  $\Delta \mathbf{w}$  is computed for each iteration of the Levenberg–

Marquardt method. However from a practical perspective, the computational complexity for calculating  $\mathbf{H}(\mathbf{w})$  is demanding especially when the dimensionality of the weight  $\mathbf{w}$  is high. This computational complexity is due to the complex nature of the Hessian  $\mathbf{H}(\mathbf{w})$ . Fortunately this difficulty is mitigated by approximating the Hessian simply as

$$\mathbf{H}(\mathbf{w}) \approx \frac{1}{N} \sum_{i=1}^N \left[ \frac{\partial F(\mathbf{x}(i), \mathbf{w})}{\partial \mathbf{w}} \right] \left[ \frac{\partial F(\mathbf{x}(i), \mathbf{w})}{\partial \mathbf{w}} \right]^T \quad (7)$$

This approximation method is recognized as the outer product of the partial derivative  $\frac{\partial F(\mathbf{w}, \mathbf{x}(i))}{\partial \mathbf{w}}$  with itself, averaged over the training sample. Clearly, the approximate version of the Levenberg-Marquardt algorithm based on the gradient vector (equation 4) and the Hessian (equation 7) is a first order method of optimization which is well suited for non-linear least square estimation problems.

The loading/blending factor  $\Lambda$  plays a very crucial role in the implementation of Levenberg-Marquardt algorithm. If the parameter  $\Lambda$  is set to 0, then equation 2 reduces to the well known traditional Newton method. However if we assign a large value to  $\Lambda$  such that  $\Lambda \mathbf{I}$  becomes more important in equation 2 compared to Hessian  $\mathbf{H}$ , then the Levenberg-Marquardt algorithm functions effectively like the gradient descent method employed in the traditionally used backpropagation algorithm. From this, we conclude that at each iteration of the algorithm, the value assigned to  $\Lambda$  should be just large enough to maintain the sum matrix  $(\mathbf{H} + \Lambda \mathbf{I})$  in a positive definite form. The specific formulation for selection of the parameter  $\Lambda$  has been proposed by [34] as follows:

- Compute  $\Omega_{av}(\mathbf{w})$  at iteration (n-1)
- Choose a modest value for  $\Lambda$ , say  $\Lambda = 10^{-3}$
- Solve equation 2 for the adjustment of  $\Delta\mathbf{w}$  at iteration (n) and evaluate  $\Omega_{av}(\mathbf{w} + \Delta\mathbf{w})$
- If  $\Omega_{av}(\mathbf{w} + \Delta\mathbf{w}) \geq \Omega_{av}(\mathbf{w})$  increase  $\Lambda$  by factor 10 or more go back to the above step.
- If  $\Omega_{av}(\mathbf{w} + \Delta\mathbf{w}) \leq \Omega_{av}(\mathbf{w})$ , decrease  $\Lambda$  by factor 10, update the trial solution  $\mathbf{w} \rightarrow \mathbf{w} + \Delta\mathbf{w}$  and go back to step 3.

An indepth comparison of the popular back-propagation (generally used in the ANN applications) and Levenberg–Marquardt method (used in the present work) has been studied in detail and the superior performance of the latter method is also demonstrated [35]. Thus, we have decided to use more efficient Levenberg–Marquardt method in the present study.

A properly trained ANN can be thought of as an expert in the category of information it has been given to analyze. Thus ANN is a massively parallel distributed processor made up of simple processing units that has a natural propensity for storing experimental knowledge and making it available for use. It is similar to the human brain functioning in the sense that the knowledge is acquired by the network from its environment through a learning process and interneuron connection strenghts, known as synaptic weights are used to store the acquired knowledge. The procedure used to acquire the knowledge is called the learning algorithm, the



Table 3: Mean Square Error (MSE) for different number of neurons used in the training of ANN.

Neurons	MSE	$\sigma(\text{Training})$	$\sigma(\text{Testing})$
3	$3.08 \times 10^{-3}$	48.7%	54.3%
4	$1.05 \times 10^{-3}$	17.1%	19.1%
5	$1.03 \times 10^{-3}$	16.6%	48.2%
10	$2.02 \times 10^{-6}$	1.97%	75.3%

function of which is to modify the synaptic weights of the network in an orderly fashion to attain the desired objective based on some well established error minimizing methods. The modification of the synaptic weights provides the traditional method for the design of the neural networks. Such an approach is closest to linear adaptive filter theory, which is well established and applied in many diverse fields.

#### 4.2. Application of ANN

In the present work, we use ANN to constrain the redshift of a sample of blazars using the combined  $\gamma$ -ray spectral measurements in GeV-TeV energy bands from *Fermi*-LAT and ground-based Cherenkov telescopes. The main objective is to predict the redshift ( $z$ ) of a blazar using the set of measured spectral indices  $\Gamma_{TeV}$ ,  $\Gamma_{3FGL}$  and  $\Gamma_{1FHL}$ . Therefore, the data set for training ANN in this work consists of 3 inputs:  $\Gamma_{TeV}$ ,  $\Gamma_{3FGL}$  and  $\Gamma_{1FHL}$  and 1 output which is the redshift ( $z$ ) of the sources to be predicted. We have used  $\sim 35$  blazars (listed in Table 1) for training the ANN. The first step towards using the Levenberg-Marquardt method, is to find the optimized number of neurons which are employed for train-

ing. A trial and error method is employed for selecting the optimized number of neurons. We started with 3 neurons in one hidden layer and changed it to 4, 5, and 10 and observed the performance of the ANN. The goodness of the performance is determined by the Mean Square Error (MSE) in each case. The MSE is defined as

$$MSE = \frac{1}{N} \sum_{i=1}^N (Y_{true}^i - Y_{pred}^i)^2 \quad (8)$$

where  $N$  is the number of samples,  $Y_{true}^i$  and  $Y_{pred}^i$  are the true and predicted (by ANN) values of the expected output for  $i$ -th example. This function is minimized during the training process for the ANN. Variation of number of neurons versus MSE is given in Table 3. It is clear from the table that the lowest MSE of  $2.02 \times 10^{-6}$  is obtained for 10 neurons. Levenberg-Marquardt algorithm being inherently a very powerful method, one has to be extremely careful to avoid any overfitting while choosing the number of neurons in the hidden layer. Overfitting of data can result due to choosing a higher number of neurons than required. This leads to the memorising of the training data rather than generalizing it. A simple method to check the overfitting is to check the results on test data which have not been seen by the network during training. The blazars used for testing from the sample are summarized in Table 2. For a good generalization the performance on test and training data should be nearly similar (slightly better results are expected for training data). The performance of ANNs with different number of neurons on the training and testing data is compared in Table 3, where columns 3 and 4 are the standard deviations ( $\sigma$ ) corresponding to the training and testing data sets

respectively. It is obvious from the table that overfitting starts after 5 neurons due to large discrepancy between the values of standard deviation for training and the testing. In view of this, there is no need to increase the number of neurons further as that would only have worsened the results. Best results were obtained with 4 neurons (row 2 in Table 3) where close matching is found between the training and the testing results. Thus 4 neurons in one hidden layer can be employed for the prediction of unknown redshifts of blazars. Next, we have to optimize the number of iterations, which happens to be a slightly easier task. Once 4 neurons are chosen, we have optimized the number of iterations using the MSE. The variation of the MSE as a function of number of iterations with 4 neurons is shown in Figure 2. We observe that the MSE does not vary after  $\sim 11000$  iterations. This suggests that approximately 15000 iterations performed for the error reduction are sufficient for the problem at hand.

## 5. Results and Discussion

In this work, we used a sample of approximately 45 blazars which have been detected at GeV energies by the *Fermi*-LAT and at TeV energies by the ground-based  $\gamma$ -ray instruments for constraining their redshifts using ANN. A close look of the test data sample listed in Table 2 (columns 3 and 4) suggests that the known redshifts of the blazars ( $z$ ) are in good agreement with the values predicted by the Levenberg - Marquardt based artificial intelligence using ANNs. The results are found to be consistent well within an uncertainty of  $\sim 18\%$  as listed under column 5 in Table 2. This indicates that the  $\gamma$ -ray spectral indices of blazars obtained

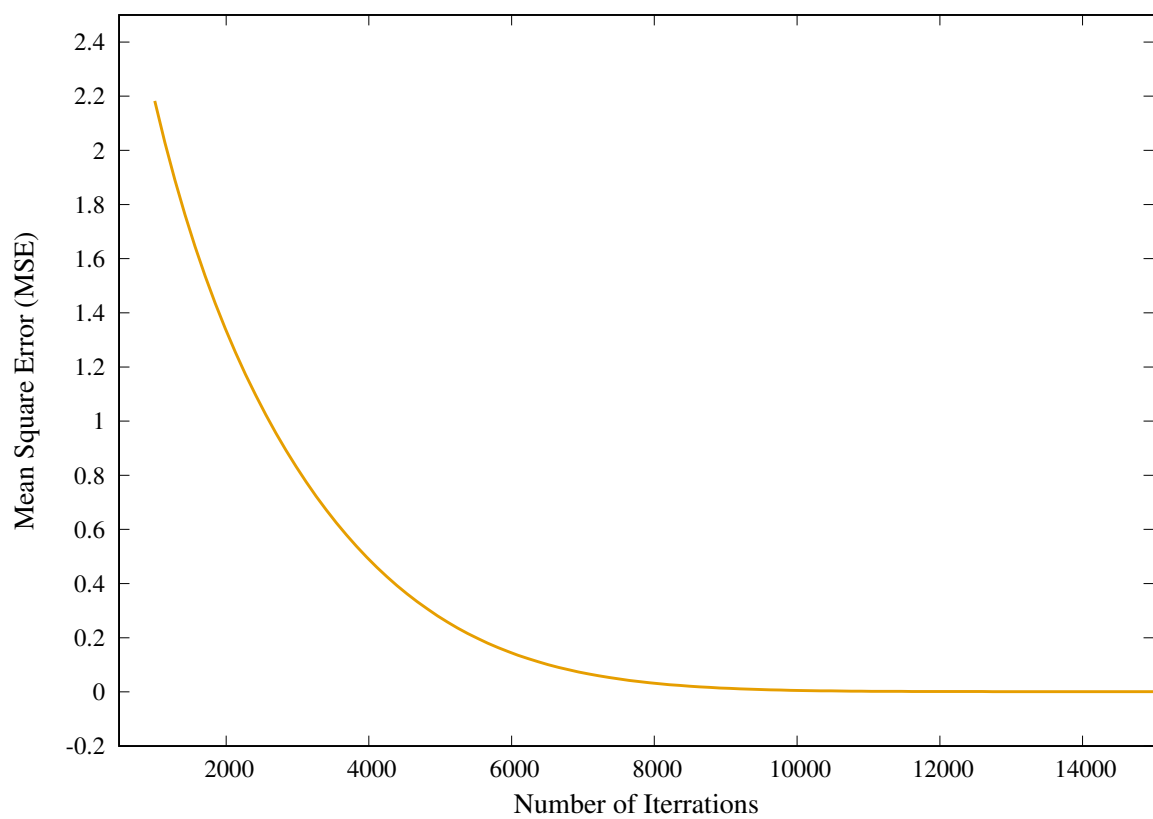


Figure 2: Optimization of the number of iterations using mean square error (MSE) estimation for LevenbergMarquardt algorithm with 4 neurons.

from the *Fermi*-LAT and ground-based VHE observations can be used to constrain or predict their redshifts with good accuracy. The  $\gamma$ -ray spectral indices shown in Figure 1 suggests that the *Fermi*-LAT spectral indices reported in 3FGL and 1FHL catalogs are nearly similar. However, the TeV spectral indices ( $\Gamma_{TeV}$ ) show significant softening with increasing redshift as compared to  $\Gamma_{3FGL}$  and  $\Gamma_{1FHL}$ . This implies a clear spectral break in the  $\gamma$ -ray spectra of blazars observed with the *Fermi*-LAT and TeV instruments. The observed  $\gamma$ -ray spectral break ( $\Delta\Gamma$ ), which is defined as the difference between the measured GeV and TeV spectral indices, is shown in Figure 3 as a function of redshift ( $z$ ). It is observed from Figure 3 that the spectral break is non-zero for all the blazars used in the sample for training and testing the ANN. For the blazar sample used in training the ANN, the observed spectral break is a linear function of the redshift ( $z$ ), which can be mathematically expressed as

$$\Delta\Gamma = \Gamma_{TeV} - \Gamma_{LAT} = az + b \quad (9)$$

where  $a$  and  $b$  are the parameters, and  $\Gamma_{LAT}$  is the spectral index measured by *Fermi*-LAT ( $\Gamma_{3FGL}$  or  $\Gamma_{1FHL}$ ). For the spectral break between  $\Gamma_{TeV}$  and  $\Gamma_{3FGL}$ , the best fit parameter values are found to be  $a = 3.78 \pm 0.74$  and  $b = 0.67 \pm 0.09$ . Similarly, for the spectral break between  $\Gamma_{TeV}$  and  $\Gamma_{1FHL}$ , we get  $a = 3.04 \pm 0.77$  and  $b = 0.60 \pm 0.11$ . This indicates that the values of parameters  $a$  and  $b$  are similar within error bars for both the cases. Therefore, the GeV spectral indices in the energy range 0.1-500 GeV and TeV spectral indices above  $\sim 100$  GeV of the

blazars lead to a redshift dependent spectral break in their  $\gamma$ -ray spectra. The origin of the observed spectral break in the  $\gamma$ -ray spectra of blazars is not clearly known and is attributed to several factors like an intrinsic break in the emitted spectrum of the source (intrinsic curvature) or softening of the TeV spectrum due to EBL absorption (extrinsic curvature) in the extragalactic space [36, 37]. The attenuation of TeV  $\gamma$ -ray photons during the propagation from source to Earth via  $\gamma_{TeV}\gamma_{EBL} \rightarrow e^-e^+$  strongly depends on the local density of EBL photons and redshift of the source. Therefore, any uncertainty in the EBL photon density will lead to the incorrect estimation of the spectral break as investigated by [17]. Also the intrinsic curvature in the emitted spectrum depends on the particle distribution considered in a given blazar emission model [22]. However, the artificial intelligence methodology used in the present work is entirely based on the observed spectral break in GeV-TeV spectra of blazars and does not consider any physical effect for the curvature. The observed  $\gamma$ -ray spectral break is found to be a distinct property of blazars but its redshift evolution has not been properly explained by the blazar physics. It can provide important information about the location and structure of the  $\gamma$ -ray emission region in the blazar jet.

## 6. Summary

We have demonstrated that the spectral break observed in the GeV-TeV  $\gamma$ -ray spectra of blazars can be effectively utilised to constrain their redshift by using an ANN based artificial intelligence technique. We find that an ANN with 4 neurons in the hidden layer and with 15000 iterations can perform very well for constraining

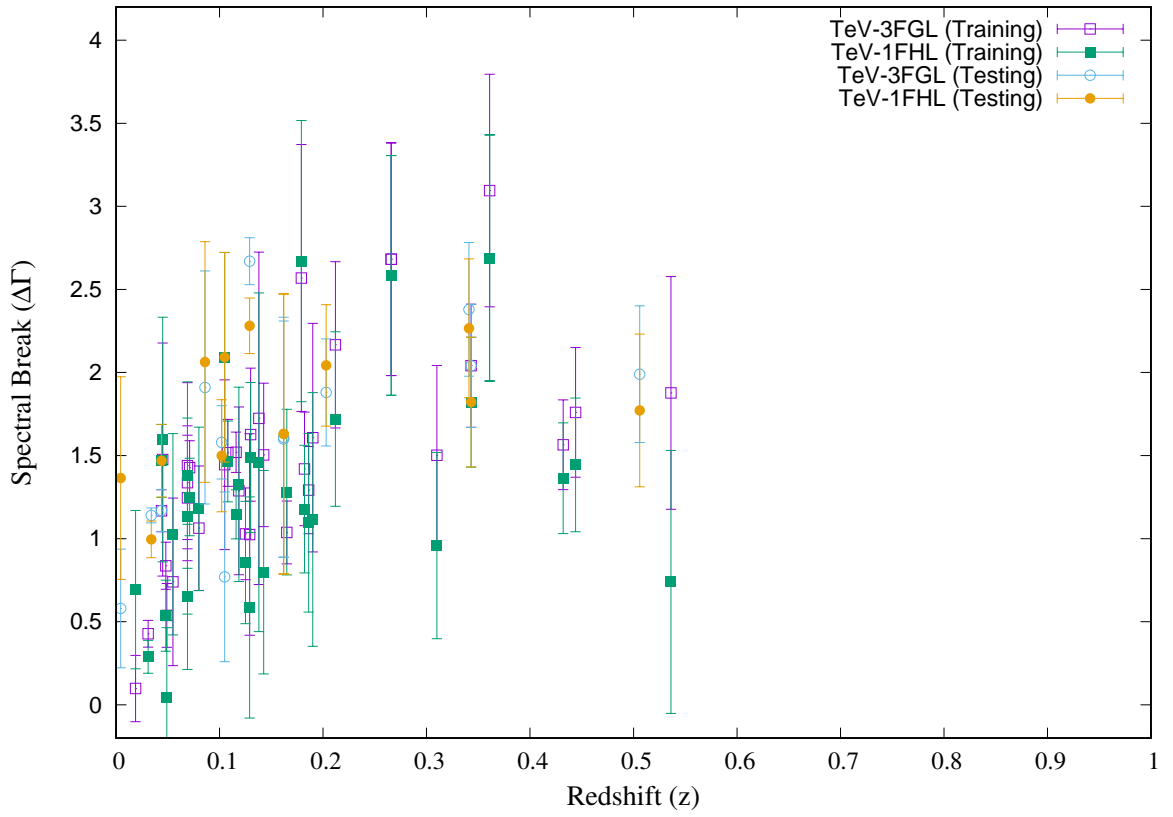


Figure 3: Spectral break between the TeV and MeV-GeV  $\gamma$ -ray spectra as a function of redshift for the blazar sample used in the ANN training and testing.

the redshift of blazars using the Levenberg-Marquardt algorithm. This technique only depends on the observational features of the  $\gamma$ -ray spectra of blazars in different energy bands. The redshift of blazars can be constrained or predicted by this technique with an uncertainty of about 18% using only the  $\gamma$ -ray spectral information from the *Fermi*-LAT and ground-based observations. The availability of more blazars in the training sample of ANN will reduce the uncertainty in the predicted values. Therefore, the results from the upcoming CTA (Cherenkov Telescope Array) observatory will be very useful for such applications based on artificial intelligence approach.

## Acknowledgments

Part of this work is based on archival data, software or online services provided by the Space Science Data Center -ASI.

## References

- [1] C. M. Urry & P. Padovani, 1995, *PASP*, 107, 803
- [2] M. Lister et al., 2018, *ApJS*, 234, 12
- [3] D. Blinov et al., 2016, *MNRAS*, 457, 2252
- [4] F. Tavecchio et al., 1998, *ApJ*, 509, 608
- [5] F. A. Aharonian, 2000, *NewA*, 5, 337
- [6] M. Böttcher et al., 2013, *ApJ*, 768, 54



- [7] A. Zech et al., 2017, *A&A*, 602, 25
- [8] A. A. Abdo et al., 2010, *ApJ*, 716, 30
- [9] E. T. Meyer et al., 2011, *ApJ*, 740, 98
- [10] P. Padovani & P. Giommi, 1995, *ApJ*, 444, 567
- [11] P. Giommi et al., 2012, *MNRAS*, 429, 2899
- [12] S. Piranomonte et al., 2007, *A&A*, 470, 787
- [13] M. S. Shaw et al., 2013, *ApJ*, 764, 135
- [14] S. Paiano et al., 2017, *ApJ*, 837, 144
- [15] M. S. Shaw et al., 2012, *ApJ*, 748, 49
- [16] Y. Yoshi et al., 2014, *ApJ*, 784, 11
- [17] E. Prandini et al., 2010, *MNRAS*, 405, 76
- [18] A. Domínguez et al., 2013, *ApJ*, 770, 77
- [19] K. K. Singh et al., 2014, *NewA*, 27, 34
- [20] A. Franceschini & G. Rodighiero, 2017, *A&A*, 603, 2017
- [21] The Fermi-LAT Collaboration., 2018, *Science*, 362, 1031
- [22] L. Qin et al., 2018, *MNRAS*, 473, 3755
- [23] G. E. Romero et al., 2012, *SSRv*, 207, 5

- [24] W. B. Atwood et al., 2009, ApJ, 697, 1071
- [25] F. Acero et al., 2015, ApJS, 218, 23
- [26] M. Ackermann et al., 2013, ApJS, 209, 34
- [27] A. Carosi et al., 2015, ICRC, 34, 757
- [28] A. A. Abdo et al., 2010, ApJ, 710, 1271
- [29] R. Sinkus, 1995, NIM A, 361, 290
- [30] V. K. Dhar et al., 2010, Pramana, 74, 307
- [31] W. McCulloch & W. Pitts, 1943, Bulletin of Mathematical Biophysics, 5, 115
- [32] V. K. Dhar et al., 2013, NIM A, 708, 56
- [33] D. E. Rumelhart et al., 1986, Nature, 323, 533
- [34] W. H. Press & D. N. Spergel, 1988, ApJ, 325, 715
- [35] V. K. Dhar et al., 2010, Measurement Science and Technology, 21, 015112
- [36] F. W. Stecker et al., 1992, ApJ, 390, 49
- [37] F. W. Stecker et al., 2006, ApJ, 648, 774